

Contents lists available at ScienceDirect

# Journal of Energy Chemistry





http://www.journals.elsevier.com/

# Enhanced capacity to CO<sub>2</sub> sorption in humid conditions with a K-doped biocarbon

Nausika Querejeta, Fernando Rubiera, Covadonga Pevida\*

Instituto Nacional del Carbón, INCAR-CSIC, c/Francisco Pintado Fe 26, 33011 Oviedo, Spain

#### ARTICLE INFO

Article history:
Received 18 July 2018
Revised 24 September 2018
Accepted 29 September 2018
Available online 18 October 2018

Keywords: Biocarbon K<sub>2</sub>CO<sub>3</sub> CO<sub>2</sub> sorption Humid flue gas

#### ABSTRACT

Solid sorbents with enhanced capacity and selectivity towards  $CO_2$  are crucial in the design of an efficient capture process. Among the possible alternatives,  $K_2CO_3$ -doped activated carbons have shown high  $CO_2$  capture capacity and rapid carbonation reaction rate. In this work, a sustainable and low-cost approach is developed with a biomass-based activated carbon or biocarbon as support. The  $CO_2$  capture performance in cyclic sorption–desorption operation and the sorption kinetics have been investigated under different scenarios in a purpose-built fixed-bed set-up. Independent of the  $H_2O$  concentration in the flue gas, a constant relative humidity ( $\sim 20\%$ ) in the  $K_2CO_3$ -doped biocarbon bed promoted the carbonation reaction and boosted the  $CO_2$  sorption capacity (1.92 mmol/g at 50 °C and 14 kPa partial pressure of  $CO_2$ ). Carbonation is slower than physical adsorption of  $CO_2$  but wise process design could tune the operation conditions and balance capture capacity and sorption kinetics.

© 2018 Science Press and Dalian Institute of Chemical Physics, Chinese Academy of Sciences. Published by Elsevier B.V. and Science Press. All rights reserved.

#### 1. Introduction

Carbon dioxide (CO<sub>2</sub>) is the dominant greenhouse gas (GHG), accounting for at least 60% of all GHG emissions, and it is an essential component of the global carbon cycle [1]. CO<sub>2</sub> is produced in large quantities as a result of fossil fuel use in power generation and industry. Fossil fuel-fired power plants are the main source of carbon dioxide emissions worldwide, contributing to approximately 40% of total global emissions. Coal-fired power plants alone contribute to approximately 70% of the emissions from fossil fuel-fired power plants [2].

Therefore, it is becoming increasingly urgent to develop efficient carbon capture technologies for controlling the CO<sub>2</sub> emissions from fossil fuel combustion at point sources like thermal power plants and steam generators. Post-combustion technologies can be retrofitted to existing facilities and, therefore, are convenient to be deployed at large scale in a short time frame. Hence, post-combustion CO<sub>2</sub> capture can offer an interim solution for CO<sub>2</sub> removal from combustion flue gases, until new clean energy generation technologies emerge [3].

Under the low  $CO_2$  partial pressure conditions found, for instance, in post-combustion flue gases the absorption/stripping process, using amine solutions such as monoethanolamine (MEA),

\* Corresponding author.

E-mail address: cpevida@incar.csic.es (C. Pevida).

is regarded as the most mature commercialized technology [4]. However, this technology presents several drawbacks that include high energy consumption, toxicity due to losses of the solvent, corrosion of the equipment, etc. Adsorption-based technologies for CO<sub>2</sub> capture entail a viable alternative due to their potential to be more energy efficient than chemical absorption.

In any adsorption-based process, adsorbate molecules are separated selectively from a gas mixture by means of a sorbent wherein the type of bonding involved depends on the pair adsorbate-sorbent. In this regard, CO<sub>2</sub> sorption can take place by means of physisorption, chemisorption, or even a mixture of both.

Flue gas from major  $CO_2$  emitters contains less than 15 vol%  $CO_2$  at temperatures above ambient and at atmospheric pressure. Non- $CO_2$  fraction composition is highly variable, although atmosphere gases are dominant. Water vapor, particularly, is a nuisance to capture  $CO_2$  given the high concentration in the flue gas. It is therefore fair to say that most research efforts on capture should be directed towards wet streams [1].

To accomplish the design of an efficient adsorption process it is mandatory to develop a proper adsorbent depending on the features of the gas streams to be treated. Designing an adsorbent for CO<sub>2</sub> capture under industrially acceptable standards focuses on the following attributes: (1) high CO<sub>2</sub> uptake, (2) high selectivity to CO<sub>2</sub>, (3) cyclability over at least 1000 cycles, (4) fast kinetics, (5) stability in water vapor and acidic gases, and (6) the adsorbent should be produced at a low cost [1].

**Table 1.** Textural characterization performed from physical adsorption of N₂ at −196 °C and of CO₂ at 0 °C.

Textural parameters		
Total pore volume	$V_{\rm p}$	Amount of N <sub>2</sub> adsorbed at a relative pressure of 0.99
Surface area	BET	Brunauer-Emmett-Teller equation [14]
Micropore volume	$W_0$	$N_2$ isotherms: Dubinin-Radushkevich (DR) equation assuming a density of the adsorbed phase of 0.808 cm $^3$ g $^{-1}$
Micropore surface area	$S_{\mathrm{DR}}$	and a cross sectional area of 0.162 nm <sup>2</sup> [15]; CO <sub>2</sub> isotherms: Dubinin–Astakhov (DA) equation assuming a density of the adsorbed phase of 1.023 cm <sup>3</sup> g <sup>-1</sup> and a cross sectional area of 0.187 nm <sup>2</sup> [16]; $E_0$ , characteristic energy, and $n$ , exponent in the DA equation, only depends on the micropore system.
Average micropore width	$L_0$	Stoeckli-Ballerini equation [17]
Pore size distribution	PSD	Quenched Solid State (QSDFT) for $N_2$ isotherms and Non-local Density (NLDFT) Functional Theory for $CO_2$ isotherms, assuming slit pore model.

The capacity of conventional microporous adsorbents to adsorb  $CO_2$  decreases in wet atmospheres and at temperatures higher than 40 °C, which makes their use inefficient [5]. At low pressures and in physisorption based solids,  $H_2O$  competes with  $CO_2$  for the adsorption sites, leading to loss in uptake capacity [1].

Recently, it has been reported that dry regenerable alkali metal-based sorbents can be used to capture  $CO_2$  in flue gas from fossil fuel-fired power plants [6]. In this context, water aids the capture of  $CO_2$  by acting as a solvent and catalyst during bicarbonate formation. Thus, for such sorbents, both physisorption and chemisorption occur onto the surfaces of the sorbent and the alkali, respectively.

Among the various kinds of alkali metal-based sorbents [7–10],  $K_2CO_3$  doped AC (activated carbon) has shown high  $CO_2$  capture capacity and rapid carbonation reaction rate [11].  $K_2CO_3$  can capture  $CO_2$  from flue gas at low temperatures (40–80 °C), forming potassium bicarbonate (KHCO<sub>3</sub>) via the carbonation reaction [3]. Thus, it is very important to control the carbonation reaction rate and to tune the  $CO_2$  absorption capacity of these sorbents in order to design a suitable dry regenerable sorbent for  $CO_2$  capture [6].

With this regard, K<sub>2</sub>CO<sub>3</sub> doped biomass-based AC is proposed herein as a promising candidate for CO<sub>2</sub> capture at low temperature (50 °C) under humid flue gas conditions. The use of a biomass-based activated carbon or biocarbon as support, scarcely reported in literature, constitutes a novel, sustainable and low-cost approach. To address the potentiality and applicability of the K-doped biocarbon produced, the CO<sub>2</sub> capture behaviors, performances in eight consecutive CO<sub>2</sub> sorption–desorption cycles, and sorption kinetics of both the AC support and the K<sub>2</sub>CO<sub>3</sub>/AC in a simulated flue gas atmosphere have been investigated in a purpose-built fixed-bed unit. Further insights have been focused into the effects of water pretreatment and the carbonation reaction pathways of K<sub>2</sub>CO<sub>3</sub>/AC for CO<sub>2</sub> capture.

## 2. Experimental

# 2.1. Sorbent preparation

Activated carbon RN2 previously produced in our laboratory departing from olive stones in a single-step  $CO_2$  activation procedure [12] was selected as carbon support. This activated carbon is in granular form with average particle size of  $\sim$ 1–2 mm.

Anhydrous alkali metal carbonate,  $K_2CO_3$  (Sigma Aldrich, ACS Reagent,  $\geq 99.0\%$ ) was used as received for carbon impregnation. The dry potassium-based carbon sorbent was prepared through an impregnation method adapted from Guo et al. [13]. The preparation protocol was as follows:  $5.0\,\mathrm{g}$  of activated carbon (RN2) were added to an aqueous solution containing  $2.5\,\mathrm{g}$  of  $K_2CO_3$  in  $25\,\mathrm{cm}^3$  of distilled water. It corresponds to an impregnation ratio of 40% that has been identified as optimum [8]. Then, the content was mixed with a magnetic stirrer for  $15\,\mathrm{h}$  at room temperature. After stirring, the mixture was dried in an air oven at  $105\,^{\circ}\mathrm{C}$  during  $3.5\,\mathrm{h}$ . The dried sample was calcined in a furnace, at a slow heating rate of  $5\,^{\circ}\mathrm{C/min}$  up to  $300\,^{\circ}\mathrm{C}$ , under  $N_2$  flow  $(100\,\mathrm{cm}^3/\mathrm{min})$  and

a soaking time of 2 h was set. The resulting sample is named after RN2K, where K stands for the  $K_2CO_3$  impregnation.

#### 2.2. Sorbent characterization

#### 2.2.1. Pore structure characteristics

The porous structure of the parent activated carbon (RN2) and the potassium-based carbon (RN2K) was assessed prior to the  $\rm CO_2$  sorption–desorption experiments. The porosity of the activated carbons was fully characterized by means of physical adsorption of  $\rm N_2$  at  $-196\,^{\circ}$ C, in a Micromeritics ASAP 2010, and adsorption of  $\rm CO_2$  at 0 °C, in a Micromeritics TriStar 3000. Helium density and apparent density were measured in an Accupyc 1330 at 35 °C and in a Micromeritics Autopore IV 9500 mercury porosimeter at 0.1 MPa, respectively. The samples were outgassed at 100 °C under vacuum overnight prior to all the measurements.

The use of both adsorbates,  $N_2$  and  $CO_2$ , provides complementary information about the porous texture of the samples: the adsorption of  $CO_2$  at  $0\,^{\circ}C$  and up to atmospheric pressure is restricted to pores narrower than 1 nm, whereas  $N_2$  adsorption at  $-196\,^{\circ}C$  covers wider pore sizes but presents diffusion limitations in the narrower pores. A summary of the methodology followed in the textural characterization is included in Table 1.

# 2.2.2. Scanning electron microscopy (SEM)

The success of the impregnation method and the distribution of  $K_2CO_3$  onto the carbon precursor is another important parameter to be assessed. The particle morphology and composition of RN2K was examined by scanning electron microscopy with energy dispersive X-ray spectroscopy (SEM/EDX) in a Quanta FEG 650 equipped with an Ametek-EDAX analyzer (detector: Apollo X). The SEM images were taken at a magnification of 1500 and at 25 kV.

#### 2.3. CO<sub>2</sub> sorption behavior of the sorbents

Single  $CO_2$  sorption (breakthrough) and cyclic  $CO_2$  sorption-desorption experiments of the studied solid sorbents were performed in a purpose-built fixed-bed unit thoroughly described elsewhere [18–23].

A simulated flue gas (total flowrate of  $140\,\mathrm{cm^3/min}$ ) composed of  $14\%\,$  CO<sub>2</sub>, balance N<sub>2</sub>, was fed to a bed at  $50\,^\circ\mathrm{C}$  and atmospheric pressure. Experiments in the presence of a stream of  $\mathrm{H_2O_{(v)}}$  (0.14 g/h) in addition to  $\mathrm{CO_2}$  and N<sub>2</sub> were also conducted in order to assess the role of water vapor in the  $\mathrm{CO_2}$  sorption process from flue gas.

The total flowrate (140 cm<sup>3</sup>/min), pressure (130–140 kPa) and adsorption temperature (50 °C) were maintained constant in all fixed-bed experiments. Desorption was carried out at 70 °C and applying a light vacuum of 10 kPa, simulating vacuum-temperature swing adsorption (VTSA) operation in the cyclic experiments.

The characteristics of the beds of the two carbons evaluated are presented in Table 2.

Table 2. RN2 and RN2K bed characteristics.

Bed characteristics		RN2	RN2K
Mass of adsorbent	(g)	4.39	5.19
Total porosity	-	0.87	0.81
Helium density	(g/cm <sup>3</sup> )	2.10	2.10
Apparent density	(g/cm <sup>3</sup> )	0.50	0.72
Bed diameter	(cm)	1.30	1.30
Bed height	(cm)	11.90	10.00
Bed density	(g/cm <sup>3</sup> )	0.28	0.39

#### 2.3.1. Cyclic fixed-bed operation

CO<sub>2</sub> sorbents should be easy to regenerate and should keep its performance with cycling. Thus to evaluate the performances to separate CO<sub>2</sub> from simulated flue gas streams over multiple cycling, the activated carbons (ACs) were subjected to eight consecutive sorption-regeneration cycles. Each experimental run involved the following steps: preconditioning, sorption and regeneration. A detailed description is presented elsewhere [23].

Humidity contained in the flue gases negatively affects the  $\rm CO_2$  adsorption capacity of ACs due to their high affinity to moisture; however, the presence of water vapor is essential to form potassium bicarbonate from dry regenerable alkali metal-based sorbents upon reaction with  $\rm CO_2$  [24]. Thus, a different mechanism of interaction with  $\rm CO_2$  is expected for the two activated carbons under evaluation, particularly when assessed in wet conditions. To study the influence of water vapor in  $\rm CO_2$  sorption and evaluate the stability of the performances, RN2 and RN2K were subjected to other eight consecutive sorption–desorption cycles. The experimental runs included the same steps as in the dry cases but during the adsorption step a ternary mixture consisting of 14%  $\rm CO_2/84\%$   $\rm N_2/2\%$   $\rm H_2O$  was fed to the bed [23].

It is important to note that before each experiment the sorbent bed was dried by flowing  $N_2$  (140 cm<sup>3</sup>/min) for 60 min at 150 °C and atmospheric pressure.

# 2.3.2. Breakthrough experiment in water vapor pre-saturated bed

As explained above in Section 2.3.1, the presence of moisture in the flue gas stream leads to a decrease in the  $CO_2$  adsorption capacity of an activated carbon due to co-adsorption of  $H_2O$  but it is mandatory to the carbonation process of dry regenerable alkali metal-based sorbents. Therefore, to evaluate the effect of  $H_2O$  on  $CO_2$  sorption performance, breakthrough non-cyclic experiments feeding a ternary gas mixture composed of 14%  $CO_2/84\%$   $N_2/2\%$   $H_2O$  were carried out over extended time (several hours) till saturation of the bed with  $H_2O$ .

Since high concentrations of water vapor are beneficial for improving the carbonation reaction activity, a way suggested to reach effective  $CO_2$  sorption performance is to increase the carbonation conversion and reaction kinetics including water pretreatment prior to  $CO_2$  sorption [25,26]. To investigate the effect of this pretreatment, the bed was initially saturated with  $H_2O$  by feeding a gas stream containing 98%  $N_2$  and 2%  $H_2O$ . Afterwards, ternary  $CO_2/N_2/H_2O$  breakthrough curves (non-cyclic experiments) were obtained similarly to the long experiments with a fresh bed.

# 2.4. Theory/calculation

The design of a sorption process is not fully addressed with equilibrium data; sorption kinetics are also required.

#### 2.4.1. CO<sub>2</sub> adsorption kinetics

In physical-based sorption, commonly denoted as adsorption, diffusion of adsorbate molecules into the adsorbent particles is the rate controlling step.

Table 3. Adsorption kinetics models.

Kinetic model	Equation	Differential form
Pseudo-first order Avrami	$q_t = q_e(1 - e^{-k_f t})$ $q_t = q_e(1 - e^{(-(k_A t)^{n_A})})$	$ \frac{\frac{\mathbf{d}q_{\mathbf{t}}}{\mathbf{d}t} = k_{\mathbf{f}} (q_{\mathbf{e}} - q_{\mathbf{t}})  \frac{\mathbf{d}q_{\mathbf{t}}}{\mathbf{d}t} = k_{\mathbf{A}}^{n_{\mathbf{A}}} t^{n_{\mathbf{A}}-1} (q_{\mathbf{e}} - q_{\mathbf{t}}) $

Table 4. Goodness of fitting of the kinetic models.

	Equation
Sum of squared errors (SSE)  Coefficient of determination $(R^2)$	$\begin{split} SSE(\%) &= \sqrt{\frac{\sum (q_{t.exp} - q_{t.pred})^2}{N}} \times 100 \\ R^2 &= 1 - (\frac{\sum_{l=1}^{N} (q_{t.exp} - q_{t.pred})^2}{\sum_{l=1}^{N} (q_{t.exp} - q_{t.exp})^2}) (\frac{N-1}{N-p}) \end{split}$

To describe the adsorption process quantitatively and identify the adsorption mechanism, a number of adsorption kinetic models have been developed [27]. Based on a previous work [28], two models will be considered herein to describe the  $\rm CO_2$  adsorption behavior of RN2 and RN2K under the different moisture conditions evaluated: pseudo-first-order [29] and Avramiś fractional [30] models.

Table 3 shows the list of equations associated to these kinetic models, where t is the time elapsed from the beginning of the adsorption process,  $q_t$  (mmol/g) is the amount adsorbed at a given time,  $q_e$  (mmol/g) represents the amount adsorbed at equilibrium,  $k_f$  (min<sup>-1</sup>) is the pseudo-first-order rate constant,  $k_A$  (min<sup>-1</sup>) is the Avrami's kinetic constant and  $n_A$  is the Avrami's exponent.

Furthermore, to measure the discrepancy between the measured data and the predictions from the model, the sum of squared errors (SSE) [25] and the coefficient of determination ( $R^2$ ) [27,28] were estimated. Equations are shown in Table 4, where  $q_{\mathbf{t,exp}}$  and  $q_{\mathbf{t,pred}}$  are the experimentally measured and model-predicted adsorption capacities, respectively, N is the number of experimental data points for each sample and p is the number of parameters of the model.

## 2.4.2. CO<sub>2</sub> sorption kinetics

CO<sub>2</sub> capture on potassium-based sorbents is more likely to be a chemical-sorption based process, which involves the reaction with CO<sub>2</sub> to form bicarbonate. During this sorption process, adsorption and carbonation co-exist [7]; diffusion of CO<sub>2</sub> to the surface and into the pores, reaction with the active sites and formation of a layer of compact products are the main steps [25]. Thus, with the aim of studying the kinetics of CO2 sorption on RN2K, the Shrinking Core Model (SCM) was adopted to correlate the experimental data [31]. The basis of the SCM establishes that the solid is nonporous and it is initially surrounded by a fluid film through which mass transfer occurs between the solid particle and the bulk of the fluid. As the reaction proceeds, a layer of product (i.e., potassium bicarbonate) forms around the unreacted core. The solid particle is assumed to be spherical and it reacts with the fluid isothermally. Besides, the concentration of the reacting fluid is supposed to be constant or in excess [32].

Table 5 shows the list of equations associated to the SCM when applied to  $CO_2$  sorption on  $K_2CO_3$  doped materials, where q (mmol/g) is the total amount of  $CO_2$  captured,  $q_p$  (mmol/g) is the amount of physically adsorbed  $CO_2$  at a given time,  $M_{K_2CO_3}$  is the molecular mass of  $K_2CO_3$  (g/mol),  $\beta$  represents the  $K_2CO_3$  loading in the sorbent (being 1 for pure potassium carbonate), R (cm) is the radius of the particle,  $k_s$  is the reaction rate constant per unit of reaction interface,  $C^0_{CO_2}$  (mmol/cm³) and  $C^0_{H_2O}$  (mmol/cm³) are the initial concentrations of  $CO_2$  and  $CO_3$  and  $CO_4$  is the diffusion coefficient for  $CO_4$  in the product layer. The specific derivation of the expression can be found elsewhere [31].

Table 5. Shrinking core model equations.

Parameters	Equation
Carbonation conversion of the sorbent	$\eta = \frac{(q - q_p) \times M_{K_2 CO_3}}{\beta \times 1000} \times 100\%$
Global reaction rate	$t = \frac{R}{k_s C_{co_2} C_{H_2O}} (1 - (1 - \eta)^{\frac{1}{3}}) +$
	$\frac{{}^{C^0}_{K_2CO_3} {}^{R^2}}{{}^{6}D_{e}{}^{C^0}H_{h,O}} (1 - 3(1 - \eta)^{\frac{2}{3}} + 2(1 - \eta))$
Surface chemical reaction-controlled region	$t = A_1 g(\eta)$
	$g(\eta) = 1 - (1 - \eta)^{\frac{1}{3}}$
	$A_1 = \frac{R}{k_s C^0_{CO_2} C^0_{H_2O}}$
Internal diffusion-controlled region	$t = A_2 P(\eta)$
	$P(\eta) = 1 - 3(1 - \eta)^{\frac{2}{3}} + 2(1 - \eta)$
	$A_2 = \frac{{}^{C^0}{}_{K_2 CO_3}}{6D_e {}^{C^0}{}_{H_2 O}} {}^{R^2}$

#### 3. Results and discussion

#### 3.1. Adsorbents characterization

#### 3.1.1. Pore structure characteristics

The  $N_2$  adsorption isotherms at  $-196\,^{\circ}\text{C}$  of the carbons are shown in Fig. 1(a). Both activated carbons presented type I adsorption isotherms, according to IUPAC classification, characteristic of microporous materials. As previously explained elsewhere [12], from the open elbow in the low pressure range of the  $N_2$  adsorption isotherm on RN2, it is deduced that this activated carbon possesses both narrow and wider microporosity. Wider micropore size distribution is suitable to impregnate an activated carbon. On the other hand, RN2K shows an isotherm with a slightly sharper elbow than RN2 that suggests narrower pore size distribution (PSD). Moreover, micropore size distribution slightly shifts to smaller micropores after impregnation (see Fig. 1b).

The  $CO_2$  adsorption isotherms of the samples at  $0\,^{\circ}C$  are represented in Fig. 2(a). Comparison of the volumes adsorbed of both adsorbates,  $N_2$  and  $CO_2$ , gives an indication of the micropore ratio in each sample. Both activated carbons show similar PSD in the narrow microporosity domain (Fig. 2b). Table 6 summarizes the textural parameters estimated from the adsorption isotherm data.

The impregnation of RN2 with potassium carbonate notably reduces the volume of available porosity for  $N_2$  and  $CO_2$  adsorption. Micropore surface areas ( $S_{mi}$ ) estimated from both  $N_2$  and  $CO_2$  isotherms decrease 26% and 22%, respectively, while reduction in micropore volumes ( $W_0$ ) accounts for 37% and 32%, respectively.

RN2K shows an average narrow micropore size of  $0.69 \,\mathrm{nm}$ , which has been pointed out as very suitable for  $\mathrm{CO}_2$  adsorption at post-combustion capture conditions [33–39]. However, even though it has been demonstrated that pore size governs  $\mathrm{CO}_2$  adsorption at low pressures [33–37], the reduction of the narrow micropore volume ( $W_0$ , $\mathrm{CO}_2$ ) certainly penalizes the adsorption of  $\mathrm{CO}_2$  on RN2K.

Therefore, it can be inferred that impregnation with  $K_2CO_3$  tends to block the porosity of the parent carbon to some extent, reducing notably the capacity to adsorb  $N_2$  and  $CO_2$ . This blockage largely occurs on the wider micropores (see Fig. 1b) and it has been attributed by Hayashi et al. [8] to the hydrophobicity of the carbon surface that repels droplets of aqueous potassium carbonate that move toward the wider end of the pore space.

# 3.1.2. Scanning electron microscopy (SEM)

To gather more insights into the characteristics of RN2K it was analyzed by SEM/EDX to assess the effect of impregnation with  $K_2CO_3$ .

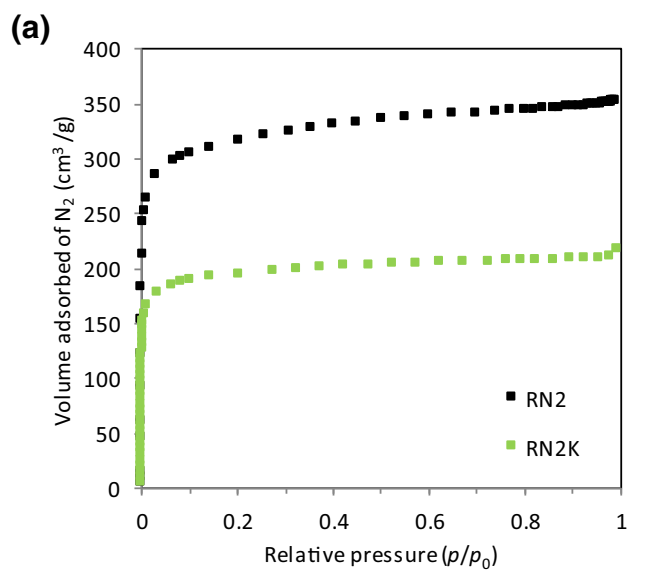
Fig. 3 shows the morphology of RN2K characterized by small white aggregates with average sizes of less than  $10\,\mu m$  that are homogeneously dispersed in the carbon structure. These white aggregates correspond to  $K_2CO_3$  as confirmed by EDX analysis (inset in Fig. 3). EDX shows high intensity potassium peak in carbon RN2K but also indicates the presence of lower intensities of C and O in the sorbent.

#### 3.2. CO<sub>2</sub> sorption performance of the RN2 ACs

#### 3.2.1. Cyclic fixed-bed operation

Stability of a  $CO_2$  sorbent in long-term cyclic operation is crucial. Thus to evaluate the performances of RN2 and RN2K in multiple cycle operation, different scenarios were considered: separation of  $CO_2$  from  $CO_2/N_2$  and from  $CO_2/N_2/H_2O$  gas streams. The  $CO_2$  sorption capacities of RN2 and RN2K during 8 consecutive cycles of sorption-regeneration were compared. The sorbents were allowed to reach  $CO_2$  saturation (maximum sorption capacity) during the sorption step and they were practically fully regenerated during the desorption step. Under humid conditions,  $H_2O$  sorption was also evaluated.

A mass balance was applied to the bed in each sorptiondesorption cycle to calculate the specific amount of CO<sub>2</sub> retained



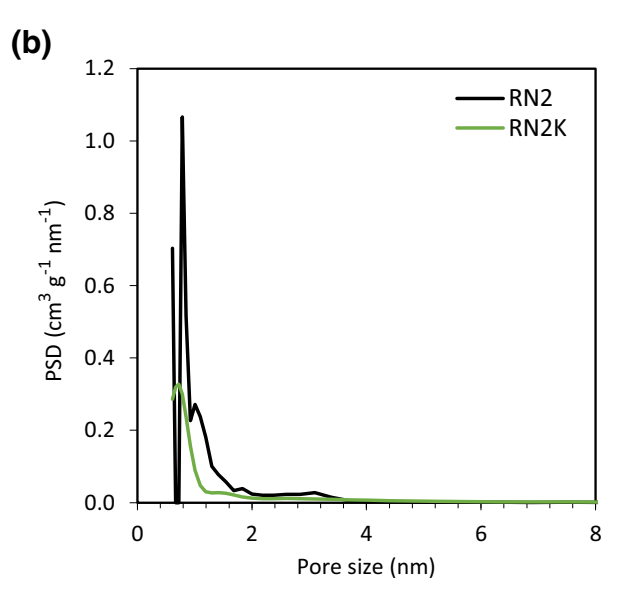
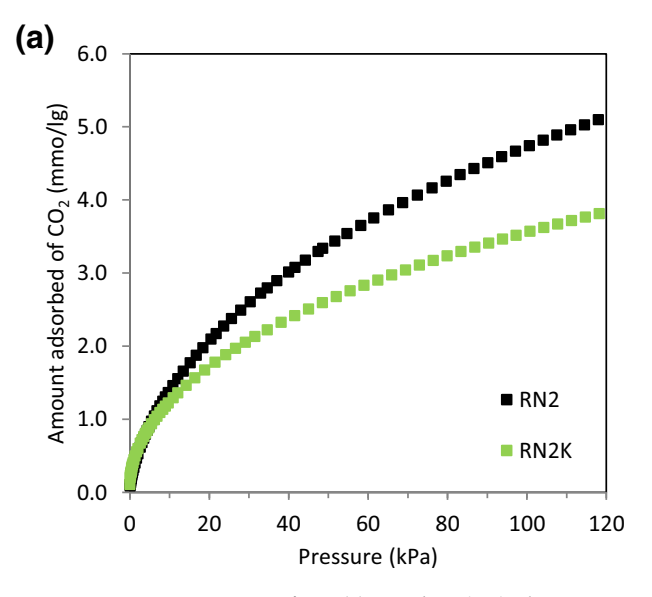


Fig. 1. (a)  $N_2$  adsorption isotherms at -196 °C and (b)  $N_2$  adsorption QSDFT PSD of RN2 ACs.



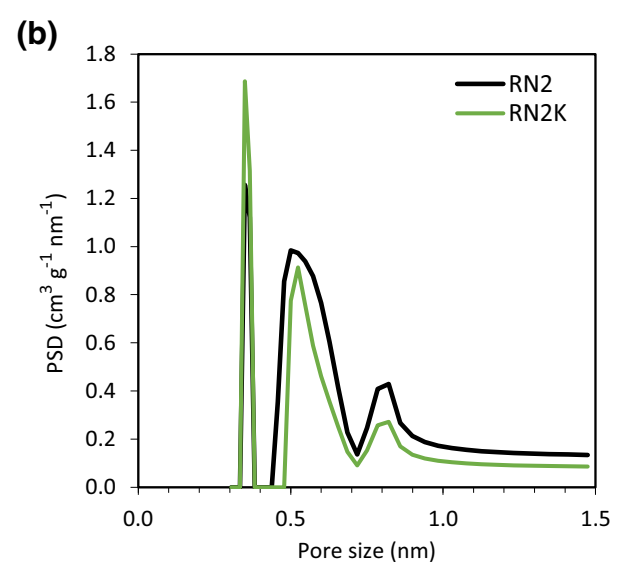


Fig. 2. (a) CO<sub>2</sub> adsorption isotherms at 0 °C and (b) CO<sub>2</sub> adsorption NLDFT PSD of RN2 ACs.

Table 6. Textural parameters of the RN2 ACs as estimated from the N2 and CO2 adsorption isotherms.

Sample	$N_2$ adsorption (-196 °C)				CO <sub>2</sub> adsorption (0 °C)						
	$\overline{V_{\rm p}}^{\rm a}$	S <sub>BET</sub> b	$W_0$ a	E <sub>0</sub> c	$L_0$ d	S <sub>mi</sub> b	n	$W_0$ a	E <sub>0</sub> c	L <sub>0</sub> d	S <sub>mi</sub> b
RN2	0.53	1248	0.48	21.3	1.09	888	1.7	0.44	24.9	0.80	1112
RN2K	0.34	768	0.30	23.1	0.92	657	1.6	0.30	27.0	0.69	868

- <sup>a</sup> V, W in cm<sup>3</sup>/g.
- $^{\rm b}$  S in  ${\rm m^2/g}$ .
- c Eo in kJ/mol.
- <sup>d</sup>  $L_0$  in nm.

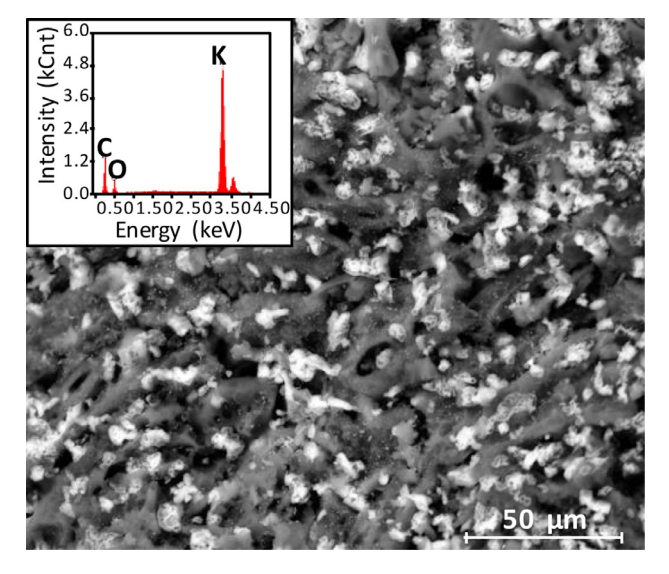


Fig. 3. SEM image of the impregnated carbon RN2K.

in the bed and the holdup of the gas phase was discounted applying correction factors. Detailed information about the calculation procedure can be found in Ref. [19].  $\rm H_2O$  sorption is significantly slower than  $\rm CO_2$ ; however, a similar calculation procedure was followed to estimate the total amount of  $\rm H_2O$  uptake at the time when the bed reached saturation in  $\rm CO_2$ .

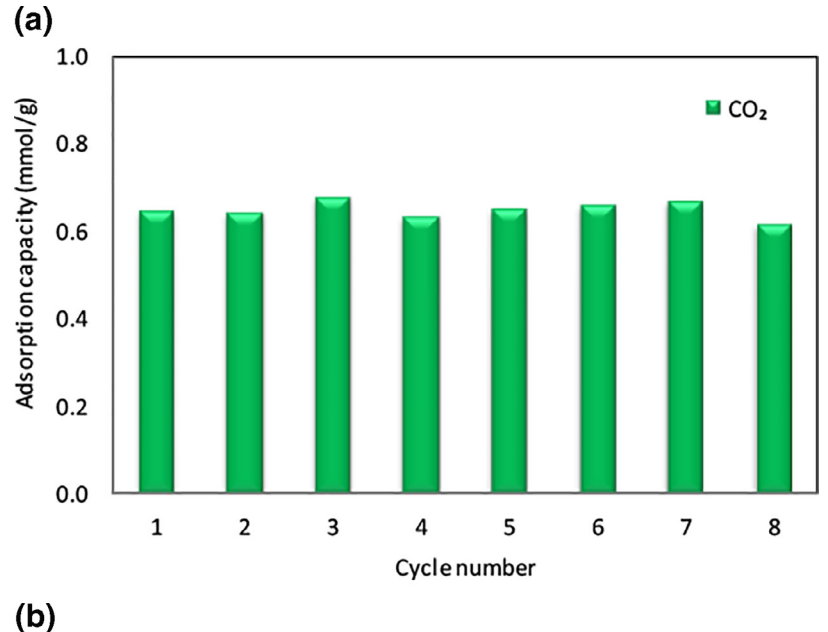
Fig. 4 plots the  $CO_2$  and  $H_2O$  adsorption capacities of RN2 for the eight consecutive cycles during the binary  $(CO_2/N_2)$  and ternary  $(CO_2/N_2/H_2O)$  experiments.

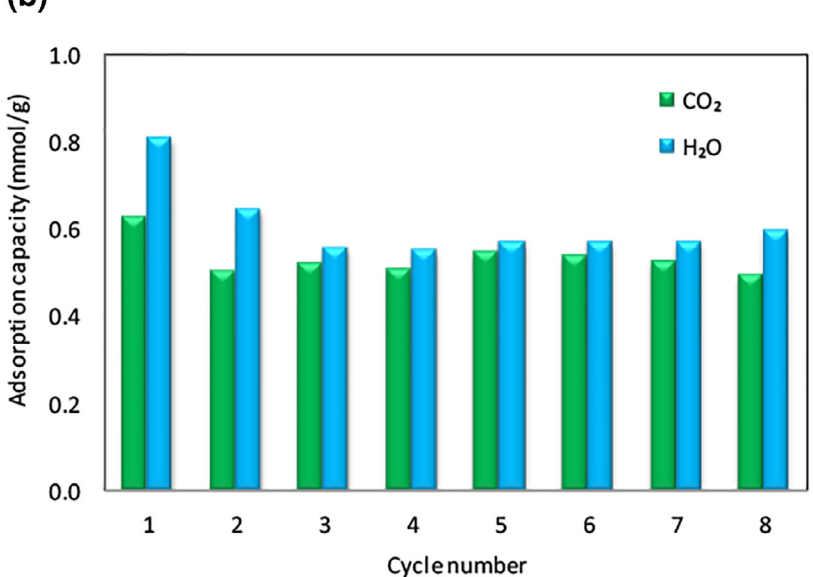
Table 7. CO<sub>2</sub> and H<sub>2</sub>O sorption capacities (average 4–8 cycles).

Sample	Feed gas	CO <sub>2</sub> sorption capacity (mmol/g)	H <sub>2</sub> O sorption capacity (mmol/g)
RN2	$CO_2/N_2$	0.63	_
	$CO_2/N_2/H_2O$	0.52	0.53
RN2K	$CO_2/N_2$	0.50	-
	$CO_2/N_2/H_2O$	0.41	0.53

As can be seen from Fig. 4(a), the  $CO_2$  adsorption capacity of RN2 is maintained over the eight consecutive cycles (0.65 mmol/g in cycle 1 and 0.62 mmol/g in cycle 8), indicating that the sorbent keeps considerable long-term working stability and cyclability. The same trend is observed for  $H_2O$  adsorption (Fig. 4b) with the exception of the first cycle. It has to be borne in mind that the bed is fully regenerated at the beginning of the first cycle and  $H_2O$  adsorption and desorption are significantly slower. This implies that  $H_2O$  is not fully removed from the bed at the beginning of each intermediate cycle. Thus, for comparative purposes among the different experiments, the capture capacity was evaluated hereafter as an average of the sorption performance over the last five cycles (cycles 4–8) in which concentrations of both  $CO_2$  and  $H_2O$  can be considered stable [23]. Results are shown in Table 7 for samples RN2 and RN2K.

Despite the doping with potassium carbonate, sample RN2K exhibits a much lower  $\mathrm{CO}_2$  uptake (reduction of 21% on average for the experiments under dry and wet conditions) when compared to RN2. This could be expected for the experiments in dry conditions, where the textural properties of the carbon play a significant role, due to prevalence of physical adsorption, and the impregnated sample needs to offset the substantial reduction in micropore





 $\textbf{Fig. 4.} \ \, \text{Adsorption capacities of RN2 in multiple cycles: (a) } \ \, \text{CO}_2/N_2 \ \, \text{and (b) } \ \, \text{CO}_2/N_2/H_2O \ \, \text{experiments.}$ 

volume. However, the sorption capacities from the ternary experiments  $(CO_2/N_2/H_2O)$  revealed that the presence of moisture penalized the  $CO_2$  uptakes of both carbons similarly. This phenomenon could be a result of the combination of the following two factors: the different kinetics of sorption of  $CO_2$  and  $H_2O$  and, most importantly, the absence of carbonation reaction due to a low  $H_2O/CO_2$  ratio (1:6) [6] or to insufficient relative humidity during the cycles [11,38]. For this reason, further experiments were conducted in the presence of water vapor to gain more insights into the role of water vapor on  $CO_2$  sorption on RN2K.

#### 3.2.2. Breakthrough experiments in humid conditions

To assess the effect of  $H_2O$  concentration on carbonation, breakthrough experiments were carried out over extended time (several hours) feeding a ternary mixture composed of 14%  $CO_2$ , 84%  $N_2$  and 2%  $H_2O$  to the bed at 50 °C and atmospheric pressure. These non-cyclic experiments departed from a fully regenerated sorbent and reached saturation of the bed with  $H_2O$ .

As can be seen in Fig. 5(a), the  $H_2O$  profiles took longer times to break through the bed: 60 and 148 min for RN2 and RN2K, respec-

Table 8. CO<sub>2</sub> and H<sub>2</sub>O sorption capacities in humid breakthrough experiment.

Sample	CO <sub>2</sub> sorption capacity (mmol/g)	H <sub>2</sub> O sorption capacity (mmol/g)
RN2	0.62	1.92
RN2K	0.49	4.09

tively. This difference in adsorption time is translated into larger  $H_2O$  sorption capacities for the potassium carbonate based sorbent RN2K (113% greater capacity than RN2, see Table 8).

Despite the sharp increase in  $H_2O$  uptake,  $CO_2$  broke through the bed in the first minutes of the experiment ( $\sim 2$  min), as can be observed in Fig. 5(b), and the  $CO_2$  sorption capacities remained unaltered for both carbons, showing the same value as that previously reported for cycle 1 of the multiple cycle experiments with a ternary gas mixture (Table 8).

This result corroborates the performance of the parent carbon RN2 in multiple cycling, where only physical adsorption of  $CO_2$  was observed. However, a different pattern would have been

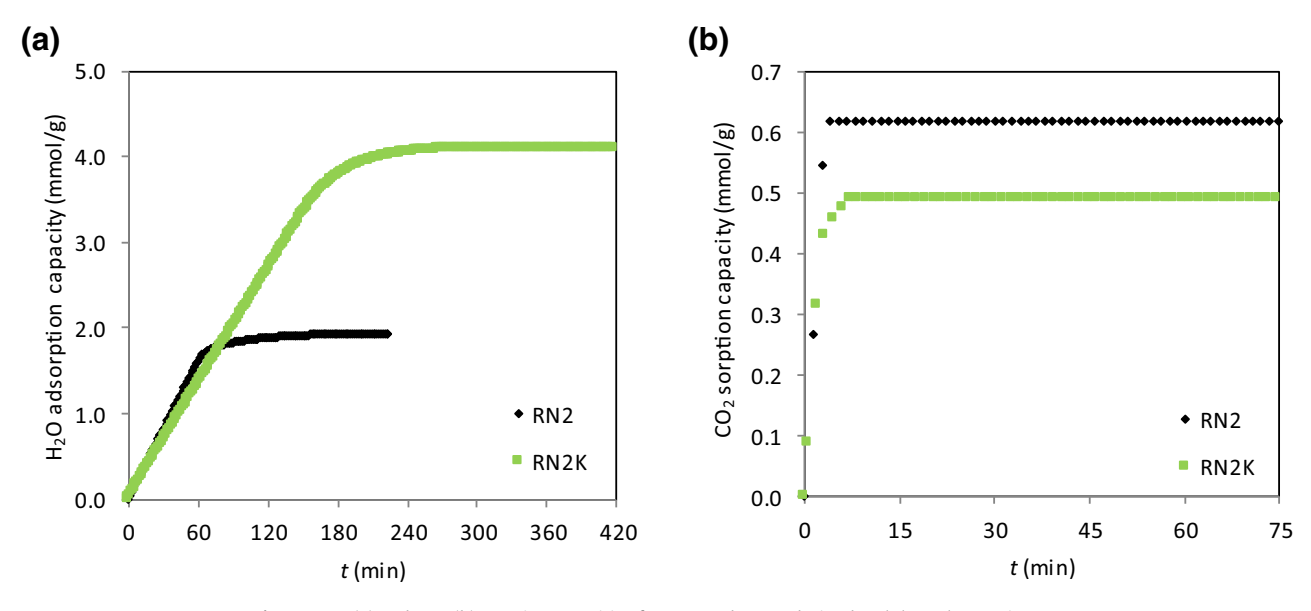


Fig. 5. H<sub>2</sub>O (a) and CO<sub>2</sub> (b) sorption capacities for RN2 and RN2K during breakthrough experiments.

expected for the potassium carbonate based sorbent, RN2K, given that the bed was allowed to reach saturation in  $H_2O$ .

Chemical sorption of  $CO_2$  on potassium carbonate based solid sorbents rely on the carbonate as the active phase to form potassium bicarbonate (KHCO<sub>3</sub>) through the following carbonation reaction (1):

$$K_2CO_3(s) + H_2O(g) + CO_2(g) \leftrightarrow 2KHCO_3(s) \tag{1}$$

However, CO<sub>2</sub> sorption does not take place straightaway via reaction 1, the following reaction steps may coexist [39]:

$$K_2CO_3(s) + 1.5H_2O(g) \leftrightarrow K_2CO_3 \cdot 1.5H_2O(s)$$
 (2)

$$K_2CO_3 \cdot 1.5H_2O(s) + CO_2(g) \leftrightarrow 2KHCO_3(s) + 0.5H_2O(g)$$
 (3)

$$2K_{2}CO_{3}(s) + 2.5H_{2}O(g) + CO_{2}(g) \leftrightarrow K_{4}H_{2}(CO_{3})_{3} \cdot 1.5H_{2}O(s) \eqno(4)$$

$$\label{eq:K4H2} \begin{array}{l} K_4 H_2 (CO_3)_3 \cdot 1.5 H_2 O(s) + \ CO_2 (g) \\ \leftrightarrow 2 \\ \text{KHCO}_3 (s) + 0.5 \\ H_2 O(g) \end{array} \tag{5}$$

Jayakumar et al. [3] have confirmed that the carbonation and hydration reactions of  $K_2CO_3$  (Eqs. (1) and (2), respectively) occur as competing reversible and parallel reactions in a simulated flue gas atmosphere, whilst reaction (3) does not occur or is negligible. In reaction (4),  $K_4H_2(CO_3)_3 \cdot 1.5H_2O(s)$  is an additive combination or a partial dissolution of  $2KHCO_3(s)$  in  $K_2CO_3 \cdot 1.5H_2O(s)$  that requires both  $H_2O$  and  $CO_2$  to form.

On the other hand, it has been previously reported that the  $CO_2$  concentration has much lesser effect on the carbonation reaction paths than the  $H_2O$  concentration [6,11,40]. Zhao et al. reported that the carbonation rate for  $K_4H_2(CO_3)_3\cdot 1.5H_2O(s)$  is higher than that of  $K_2CO_3\cdot 1.5H_2O(s)$  and so the hydration reaction is considered as the rate-controlling step for the  $CO_2$  sorption process [11,41]. Moreover, the relative humidity in the bed plays a very important role. It needs to reach a sufficient level to prevent the reversal transformation of the active species to the original phase,  $K_2CO_3$  [11,26].

Taking into consideration the aforementioned, the theoretical water uptake as per 1 g of RN2K calculated from

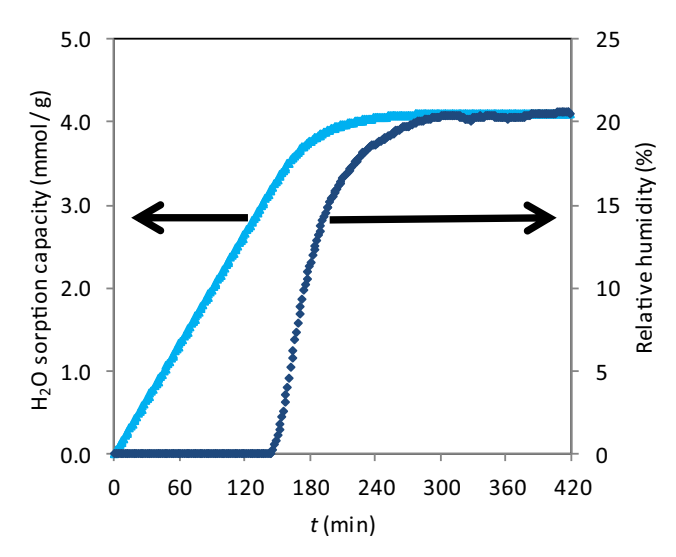


Fig. 6. Relative humidity and H<sub>2</sub>O sorption capacity profiles on RN2K.

Eq. (1) is 4.44 mmol/g. The experimental water uptake calculated from the breakthrough experiments reached 4.09 mmol/g where 1.59 mmol/g might correspond to physical adsorption of water on RN2K. The latter value is calculated departing from the uptake of the parent carbon RN2 (see Table 8) and subtracting the water vapor adsorption difference between RN2 an RN2K ( $\sim$  17%) as estimated from the first cycle of the wet cyclic experiments. Hence around 2.50 mmol/g of H<sub>2</sub>O represent the amount of water available to convert K<sub>2</sub>CO<sub>3</sub> into the intermediate K<sub>2</sub>CO<sub>3</sub>·1.5H<sub>2</sub>O(s). This value only accounts for half (56%) of the theoretical value and, consequently, it may be insufficient to allow K<sub>4</sub>H<sub>2</sub>(CO<sub>3</sub>)<sub>3</sub>·1.5H<sub>2</sub>O(s) formation (Eq. (4)).

During the breakthrough non-cyclic experiment, the relative humidity does not remain constant. It increases up to saturation of the bed in  $H_2O$  and so does the water uptake. The maximum relative humidity achieved in the gas phase was around 20%. For approximately 160 min, the relative humidity in the gas exiting the RN2K bed is negligible due to  $H_2O$  being mainly adsorbed on the bed (See Fig. 6). The unavailability of water vapor hinders the hy-

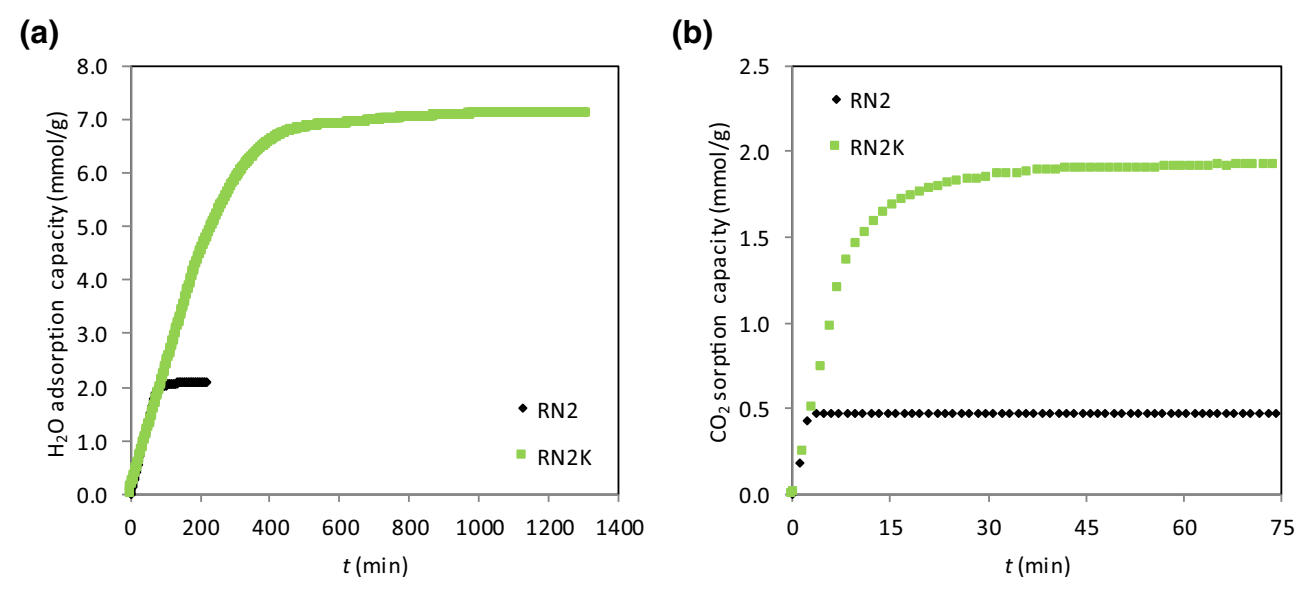


Fig. 7. H<sub>2</sub>O (a) and CO<sub>2</sub> (b) sorption capacities for RN2 and RN2K with water vapor pre-saturation of the bed.

dration reaction, which is the rate limiting step, and so the carbonation process does not take place.

Thus, we can conclude that due to the low values of  $H_2O$  concentration in the feed gas (2 vol%) and the low relative humidity in the bed during the experiment, the carbonation reaction in the RN2K bed was hindered during the breakthrough experiments. This conclusion is in agreement with Lee et al. [24], that attributed the deficient conversion of  $K_2CO_3$  into  $K_2CO_3 \cdot 1.5H_2O(s)$  to the low  $H_2O$  concentration and to the equilibrium of absorption and desorption of water at low relative humidity.

3.2.3. Effect of water vapor pre-saturation of the bed on CO<sub>2</sub> sorption As explained in the previous section, carbonation of potassium carbonate based sorbents proceeds through two main steps: firstly hydration reaction occurs to form K<sub>2</sub>CO<sub>3</sub>·1.5H<sub>2</sub>O(s) (rate-controlling) and/or K<sub>4</sub>H<sub>2</sub>(CO<sub>3</sub>)<sub>3</sub>·1.5H<sub>2</sub>O(s) under moist conditions and, secondly, the intermediates react with CO<sub>2</sub> to form KHCO<sub>3</sub>. Hence, to investigate the effect of water pretreatment on the CO<sub>2</sub> sorption performances of both activated carbons, ternary CO<sub>2</sub>/N<sub>2</sub>/H<sub>2</sub>O breakthrough non-cyclic experiments were conducted departing from beds initially saturated with H<sub>2</sub>O and N<sub>2</sub>. The H<sub>2</sub>O and CO<sub>2</sub> sorption capacity profiles are plotted in Fig. 7(a, b).

 $\rm H_2O$  sorption process follows the same pattern observed in the experiments with a fully regenerated fresh bed (see Fig. 5). However, it is apparent that the  $\rm H_2O$  uptakes are enhanced for the two carbons due to the absence of  $\rm CO_2$  during the saturation stage that thereby avoids competitive adsorption. It can be noted that the  $\rm H_2O$  capture capacity for RN2K has increased very significantly given that the bed took around 1000 min to reach saturation. On the other hand, the trend in  $\rm CO_2$  sorption reversed with respect to the fresh bed breakthrough experiments: the adsorption capacity of RN2 is reduced due to co-adsorption of  $\rm H_2O$  but in the case of RN2K, conditions seem to favor chemical sorption of  $\rm CO_2$  and a significant enhancement in the  $\rm CO_2$  uptake is observed. Thus, under these conditions of saturation in water, RN2K outperforms RN2.

Physical adsorption of water (calculated as explained in Section 3.2.2) on RN2K accounts for 1.73 mmol/g. As the theoretical value for water absorption as per 1 g of RN2K is 4.44 mmol/g and the total sorption capacity of the potassium based carbon is 7.09 mmol/g (see Table 9), there is a 13% excess water. Thus, it can be deduced that the potassium carbonate present in RN2K has been converted to  $K_2CO_3 \cdot 1.5H_2O$  [11,26,39].

Table 9. H<sub>2</sub>O and CO<sub>2</sub> sorption capacities in saturated beds.

Sample	CO <sub>2</sub> sorption capacity (mmol/g)	H <sub>2</sub> O sorption capacity (mmol/g)
RN2	0.47	2.09
RN2K	1.92	7.09

The CO<sub>2</sub> adsorption capacity of RN2 has reduced in a 24% with regards to the experiment without pretreatment (Section 3.2.2). The CO<sub>2</sub> capture capacity of RN2K rapidly increased to 1.72 mmol/g  $(\sim 17 \, \text{min})$  and then slowly approached the maximum value of 1.92 mmol/g. This means that the vast majority of the sorption capacity of RN2K at these conditions relies on chemisorption in the K<sub>2</sub>CO<sub>3</sub> phase. In amine scrubbing processes where a solution with 30 wt% monoethanolamine (MEA) is frequently used [42-45], CO<sub>2</sub> absorption capacity expressed as the difference between rich and lean solvent loadings is of about 1.23 mmol CO<sub>2</sub>/g solution [42,43]. Thus, the uptake capacity of RN2K surpasses in around 56% the outstanding capacity attributed to chemical absorption in amine-based solvents. Regarding other K-based sorbents, Lee et al. [26,46,47] attained a CO<sub>2</sub> capture capacity of 1.95 mmol/g for sorbent KACI30 at 60 °C (feed gas composition: 9 vol% H<sub>2</sub>O, 1 vol% CO2) whilst Guo et al. [25] obtained a CO2 uptake of 1.18 mmol/g for KACI15 at 20 °C (feed gas composition: 2 vol% H<sub>2</sub>O, 1 vol% CO<sub>2</sub>). Even though the testing conditions selected in these works differ from those in this study, the reported CO2 uptakes corroborate the great performance of RN2K.

Despite that the  $H_2O$  concentration is not changed in the two sets of breakthrough experiments ( $2 \text{ vol}\% \ H_2O$  in the feed gas for both the fresh and the pre-saturated bed experiments), the reason for the existence of carbonation is that water vapor pretreatment increases the relative humidity in the bed of RN2K up to 20% and this value remains constant from the beginning of the experiment whilst  $CO_2$  sorption is taking place. With water vapor pretreatment, the relative humidity in the bed is enough to allow hydration of  $K_2CO_3$  to  $K_2CO_3 \cdot 1.5H_2O$ . In environments of extremely high relative humidity  $K_2CO_3$  will be more likely to be converted into  $K_4H_2(CO_3)_3 \cdot 1.5H_2O$  during the carbonation process as shown in Eq. (4) [11,24,26,48,49]. Thus, controlling water pretreatment is crucial in the performance of RN2K as  $CO_2$  sorbent: once  $K_2CO_3 \cdot 1.5H_2O$  is formed, the relative humidity needs to be high enough to prevent the transformation back from

Table 10. CO<sub>2</sub> volumetric capacities of the support RN2 and the impregnated sample RN2K when feeding CO<sub>2</sub>/N<sub>2</sub>/H<sub>2</sub>O to the bed.

Sample	Experiment	Bed initial conditions	CO <sub>2</sub> volumetric capacity (mmol/cm <sup>3</sup> )
RN2	Multicycle, average 4-8	Fresh bed-not fully regenerated in cycling	0.14
	Breakthrough experiment	Fresh bed-H <sub>2</sub> O saturation	0.17
		Water pretreatment	0.13
RN2K	Multicycle, average 4-8	Fresh bed-not fully regenerated in cycling	0.16
	Breakthrough experiment	Fresh bed-H <sub>2</sub> O saturation	0.19
		Water pretreatment	0.75

Table 11. Kinetic parameters of pseudo-first and Avrami models under the different adsorption conditions.

Sample	Experiment	Pseudo-first-order			Avrami			
		$k_{\rm f}$ (min <sup>-1</sup> )	SSE (%)	$R^2$	k <sub>A</sub> (min <sup>-1</sup> )	$n_{A}$	SSE (%)	$R^2$
RN2	CO <sub>2</sub> /N <sub>2</sub>	0.58	2.40	0.978	0.53	1.61	0.96	0.996
	$CO_2/N_2/H_2O$	0.61	2.60	0.974	0.55	1.77	1.28	0.993
RN2K	$CO_2/N_2$	0.57	1.69	0.983	0.53	1.62	0.18	1.000
	$CO_2/N_2/H_2O$	0.52	0.96	0.994	0.51	1.20	0.68	0.997

 $K_2\text{CO}_3 \cdot 1.5H_2\text{O}$  to the original phase,  $K_2\text{CO}_3$ , and to proceed with the carbonation reaction.

# 3.3. Volumetric CO<sub>2</sub> uptake capacity

The foregoing discussion evidences that the potassium carbonate based carbon RN2K shows an outstanding  $CO_2$  performance under conditions of saturation in  $H_2O$ ; meanwhile RN2 shows better behavior in dry conditions.  $CO_2$  uptakes were reported in mass basis but it is nevertheless important to address them in volume basis, especially for post-combustion capture applications wherein reduction of the carbon footprint is a major challenge. In such scenario, the  $CO_2$  uptake per given space (volume) occupied by the adsorbent (i.e., volumetric uptake) must be maximized [38].  $CO_2$  volumetric capacities of both activated carbons have been calculated departing from the uptake capacities presented previously and the bed densities shown in Table 2.

The volumetric uptakes reported in Table 10 clearly indicate that RN2K outperforms RN2 under all the humid conditions evaluated. This is mainly ascribed to its higher packing density (0.39 g/cm³). Moreover, an uptake of 0.75 mmol  $CO_2/cm³$  can be considered outstanding for a solid sorbent at 50 °C and a  $CO_2$  partial pressure of  $\sim 14$  kPa. Previous results reported for other adsorbents derived from pine sawdust (0.30 mmol  $CO_2/cm³$ ) [50] and spent coffee grounds (0.34 mmol  $CO_2/cm³$ ) [51] at 50 °C and  $CO_2$  partial pressures of  $\sim 10$  and 15 kPa, respectively, corroborate this statement.

# 3.4. CO<sub>2</sub> adsorption kinetics

To gain more insights on how the presence of water vapor can modify the kinetics of  $\mathrm{CO}_2$  adsorption on RN2 and RN2K, cycle I of the binary and ternary multicycle experiments have been assessed. Two kinetic models were considered: pseudo-first-order and Avrami's fractional models.

Fig. 8 shows the  $q_t$  vs. t plots for RN2 and RN2K under dry and wet conditions together with the predictions from pseudo-first-order and Avrami's models (Table 3). Both carbons show two-stage adsorption that corresponds to mass transfer resistances to adsorption [52,53] and to proper surface adsorption that generally is very rapid [53–56].

The values of the kinetic parameters calculated for each model and the corresponding correlation coefficients ( $R^2$ ) and associated sum of squared errors (SSE (%)) are listed in Table 11.

The pseudo-first-order model has certain limitations in fitting the CO<sub>2</sub> adsorption data on RN2 and RN2K, whilst Avrami's frac-

tional order model suitably fits the experimental data from both binary and ternary experiments, and presents the lowest values of SSE (maximum of 1.28%) and values of  $R^2$  close to unity. Therefore, compared with the pseudo-first-order kinetic model, Avrami's equation seems the most accurate approach for describing  $CO_2$  adsorption kinetics on the carbon adsorbents studied. This is in agreement with previous studies on the kinetics of  $CO_2$  adsorption on biomass based carbons [28]. In the presence of moisture, Avrami's exponent  $(n_A)$  for the support RN2 is higher due to longer contact time of the adsorbate with the adsorbent whilst under the same conditions this time is reduced for RN2K due to the existence of the hydration reaction represented in Eq. (2) [28,57–61]. This is consistent with values of the kinetic rate constants  $(k_A)$  that evidence the different adsorption rates as a function of the contact time [30].

The excellent quality of the fit of the Avrami's model to the experimental data at low and high surface coverage is most likely associated with its ability to account for complex reaction pathways [30,57,59]. Moreover, regarding the impregnated carbon RN2K, Serna-Guerrero and Sayari [57] also concluded that the best kinetic model for describing the CO<sub>2</sub> capture performance on amine-functionalized mesoporous silica was Avrami's equation.

# 3.5. CO<sub>2</sub> sorption kinetics: carbonation reaction

Since exponent  $(n_A)$  is a fractionary number and its result is attributed to multiple kinetic order of the adsorption procedure [58], and the kinetic rate constant  $(k_A)$  encompasses both chemical and physical adsorption [57], the Avrami model is unable to explain thoroughly which sorption type is occurring and so does not account for the carbonation reaction mechanism. SCM is a dedicated model for heterogeneous reaction on solid particles and might better explain the carbonation reaction on the potassium carbonate based carbon sorbent.

In Section 3.2.3 it was concluded that RN2K is an excellent  $CO_2$  sorbent when feeding a gas stream composed of 14%  $CO_2$ , 84%  $N_2$  and 2%  $H_2O$  at 50 °C and atmospheric pressure while maintaining constant relative humidity (20%) in the bed. The  $CO_2$  sorption capacity for RN2K at these conditions was 1.92 mmol/g (mass basis). Deducting the contribution from physical adsorption as estimated from the first cycle of the multicycle experiments under dry conditions (maximum capacity of 0.57 mmol/g) and considering complete conversion of  $K_2CO_3$  to KHCO<sub>3</sub>, the corresponding carbonation conversion ( $\eta$ ) of RN2K could be estimated. A value of 45.5% was obtained at the end of the experiment (see Fig. 9).

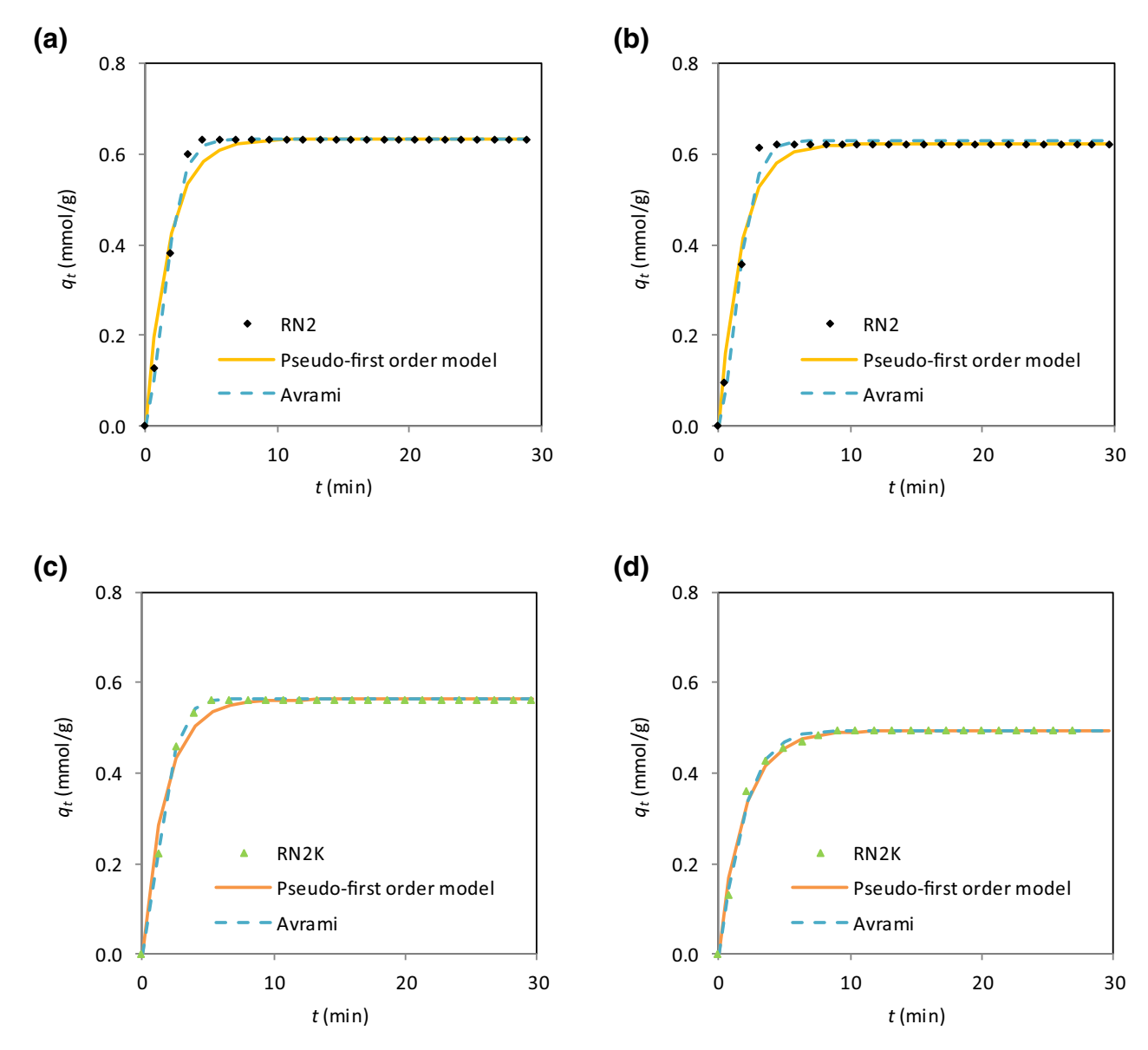


Fig. 8. Experimental and predicted  $q_t$  vs. t plots for RN2 and RN2K: binary experiments (a) and (c); ternary experiments (b) and (d).

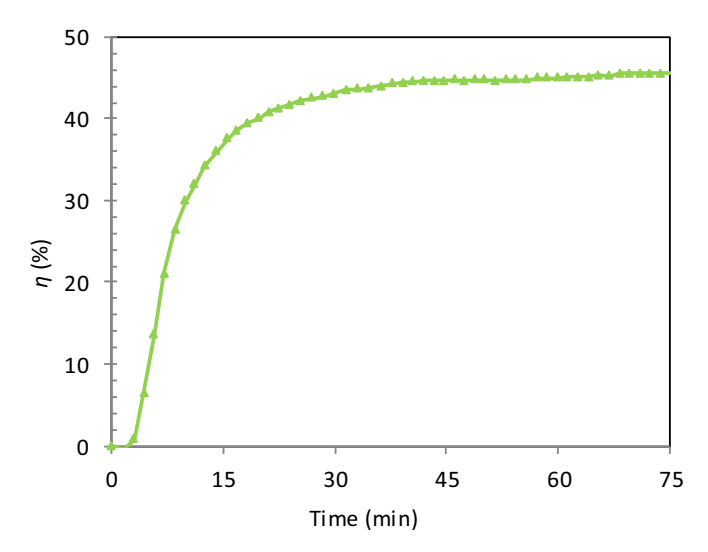
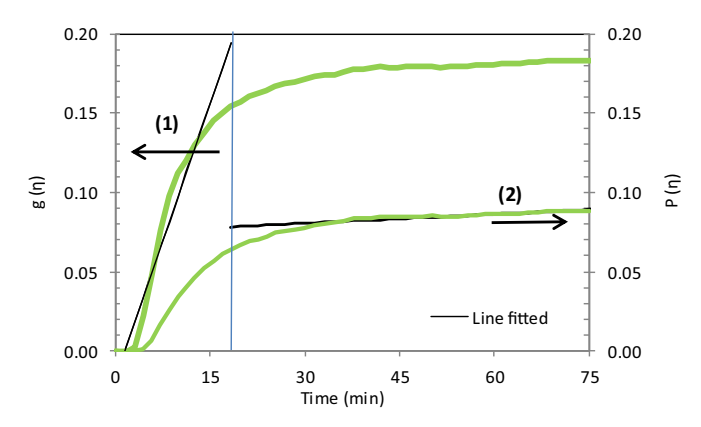


Fig. 9. Carbonation conversion of RN2K.

The carbonation conversion increases up to 38.9% with a high reaction rate (in 17 min from the start of the experiment) and then increases an additional 6.6% at a much slower pace (over the following 51 min). Hence, a different mechanism of reaction can be anticipated for each region: surface chemical reaction control during the first 17 min and internal diffusion control for the remaining duration of the experiment. Fig. 10 plots the carbonation conversion functions and the corresponding fittings to the SCM. Data were fitted independently for the two regions.

Kinetic parameters can be estimated from the slope and the intercept of the linear fittings in both regions (see Table 5). Assuming a density of  $K_2CO_3$  of 2.428 g/cm³ [31], a value of  $1.76\times10^{-2}\,\text{mol/cm}^3$  is calculated for  $C^0_{\,K_2CO_3}.$   $C^0_{\,CO_2}$  and  $C^0_{\,H_2O}$  are  $5.3\times10^{-6}\,\text{mol/cm}^3$  and  $9.4\times10^{-7}\,\text{mol/cm}^3$ , respectively. The estimated parameters are listed in Table 12.

The shrinking core model provides a good fitting of the experimental results, thus confirming the important contribution of carbonation reaction to  $CO_2$  sorption on RN2K under the conditions evaluated:  $50\,^{\circ}$ C, atmospheric pressure, feed gas composition of 14%  $CO_2$ , 84%  $N_2$  and 2%  $H_2O$  and bed initially saturated in water (RH  $\approx$  20%). Since  $1/A_1$  is two order of magnitude greater than



**Fig. 10.** Carbonation conversion of RN2K fitted to shrinking core model: (1) surface chemical reaction-controlled and (2) internal diffusion-controlled regions.

Table 12. Kinetic parameters obtained from shrinking core model.

Surface chemical reaction-controlled region			Internal diff	usion-controlle	d region
1/A <sub>1</sub> (min <sup>-1</sup> )	ks	r	1/A <sub>2</sub> (min <sup>-1</sup> )	D <sub>e</sub>	r
$1.16\times10^{v2}$	$2.25\times10^7$	0.970	$1.93 \times 10^{-4}$	$6.27\times10^{-5}$	0.979

 $1/A_2$ , these results corroborate that the carbonation conversion is mainly dependent on the first stage, the surface chemical reaction, which is the fastest [31].

#### 4. Conclusions

Potassium-based solid sorbent RN2K was prepared by impregnation with K<sub>2</sub>CO<sub>3</sub> (40%) on activated carbon RN2, a microporous based biomass carbon produced in our laboratory. Impregnation of RN2 with potassium carbonate notably reduced the volume of available porosity for adsorption. The reduction of both the narrow pore size and the narrow micropore volume in RN2K caused a slight decrease in CO<sub>2</sub> uptake when physical adsorption was the single process involved. This was the case for the dry experiments feeding CO<sub>2</sub>/N<sub>2</sub> and for the wet experiments feeding CO<sub>2</sub>/N<sub>2</sub>/H<sub>2</sub>O to a fresh bed of adsorbent. However, it was demonstrated that, independently of the H<sub>2</sub>O concentration in the feed gas, a constant relative humidity of 20% in the RN2K bed promoted the carbonation reaction and boosted the CO<sub>2</sub> sorption capacity up to approximately 2 mmol/g at 50 °C and 14 kPa partial pressure of CO<sub>2</sub>. In addition, RN2K showed outstanding performance on a volumetric basis due to its higher packing density.

The kinetics of  $\mathrm{CO}_2$  sorption on RN2K where studied from two approaches: one focused on physical adsorption and the other one on the carbonation reaction. Avrami's and Shrinking Core models suitably fitted the experimental data in each of the two cases.  $\mathrm{CO}_2$  adsorption on RN2K is however faster than carbonation.

RN2K showed stable performance upon cycling in a fixed-bed set-up and enhanced CO<sub>2</sub> capture capacity under the evaluated conditions. However, there is a trade-off between capture capacity and sorption kinetics for the potassium carbonate based carbon sorbent: carbonation leads to high capacity at the expense of slower kinetics whereas physical adsorption proceeds faster but reaches significantly lower uptakes. This opens the path for the tailoring of this material according to the process configuration design (rapid or slow cycling) and to the targets in CO<sub>2</sub> capture (CO<sub>2</sub> recovery and purity). Cycles with longer adsorption step will allow RN2K to go through carbonation reaction and so attain higher

CO<sub>2</sub> uptakes; however, regeneration over extended time will lead to higher CO<sub>2</sub> recovery but lower purity.

#### Acknowledgments

N.Q. acknowledges a fellowship from the Gobierno del Principado de Asturias (Programa Severo Ochoa).

#### References

- [1] H.A. Patel, J. Byun, C.T. Yavuz, ChemSusChem 10 (2017) 1303-1317.
- [2] J.B. Lee, T.H. Eom, B.S. Oh, J.I. Baek, J. Ryu, W.S. Jeon, Y.H. Wi, C.K. Ryu, Energy Proc. 4 (2011) 1494–1499.
- [3] A. Jayakumar, A. Gomez, N. Mahinpey, Appl. Energy 179 (2016) 531-543.
- [4] M. Wang, A. Lawal, P. Stephenson, J. Sidders, C. Ramshaw, Chem. Eng. Res. Des. 89 (2011) 1609–1624.
- [5] A.G. Okunev, V.E. Sharonov, A.V. Gubar, I.G. Danilova, E.A. Paukshtis, E.M. Moroz, T.A. Kriger, V.V. Malakhov, Y.I. Aristov, Russ. Chem. Bull. 52 (2003) 359–363.
- [6] C. Zhao, C. Zhao, X. Chen, E.J. Anthony, X. Jiang, L. Duan, Y. Wu, W. Dong, Prog. Energy Combust. Sci. 39 (2013) 515–534.
- [7] J.V. Veselovskaya, V.S. Derevschikov, T.Y. Kardash, O.A. Stonkus, T.A. Trubitsina, A.G. Okunev, Int. J. Greenh. Gas Control 17 (2013) 332–340.
- [8] H. Hayashi, J. Taniuchi, N. Furuyashiki, S. Sugiyama, S. Hirano, N. Shigemoto, T. Nonaka, Ind. Eng. Chem. Res. 37 (1998) 185–191.
- [9] Y. Guo, C. Li, S. Lu, C. Zhao, Energy Fuels 29 (2015) 8151-8156.
- [10] C. Qin, J. Yin, J. Ran, L. Zhang, B. Feng, Appl. Energy 136 (2014) 280–288.
- [11] C. Zhao, Y. Guo, C. Li, S. Lu, Chem. Eng. J. 254 (2014) 524-530.
- [12] N. Querejeta, M. Plaza, F. Rubiera, C. Pevida, Materials (Basel) 9 (2016) 359.
- [13] Y. Guo, C. Zhao, C. Li, Chem. Eng. Technol. 38 (2015) 891-899.
- [14] S. Brunauer, P.H. Emmett, E. Teller, J. Am. Chem. Soc. 60 (1938) 309-319.
- [15] F. Stoeckli, Russ. Chem. Bull. 50 (2018) 2265–2272.
- [16] H.F. Stoeckli, Carbon 19 (1981) 325-326.
- [17] F. Stoeckli, L. Ballerini, Fuel 70 (1991) 557–559.
- [18] M.V. Gil, N. Álvarez-Gutiérrez, M. Martínez, F. Rubiera, C. Pevida, A. Morán, Chem. Eng. J. 269 (2015) 148–158.
- [19] M.G. Plaza, I. Durán, N. Querejeta, F. Rubiera, C. Pevida, Ind. Eng. Chem. Res. 55 (2016) 3097–3112.
- [20] M.G. Plaza, I. Durán, N. Querejeta, F. Rubiera, C. Pevida, Ind. Eng. Chem. Res. 55 (2016) 6854–6865.
- [21] N. Álvarez-Gutiérrez, S. García, M.V. Gil, F. Rubiera, C. Pevida, Energy Fuels 30 (2016) 5005–5015.
- [22] N. Álvarez-Gutiérrez, M.V. Gil, F. Rubiera, C. Pevida, Fuel Process. Technol. 142 (2016) 361–369.
- [23] I. Durán, F. Rubiera, C. Pevida, Energies 10 (2017) 827.
- [24] S.C. Lee, B.Y. Choi, C.K. Ryu, Y.S. Ahn, T.J. Lee, J.C. Kim, Korean J. Chem. Eng. 23 (2006) 374–379.
- [25] Y. Guo, C. Zhao, C. Li, Y. Wu, Chem. Eng. J. 260 (2015) 596-604.
- [26] S.C. Lee, H.J. Chae, B.Y. Choi, S.Y. Jung, C.Y. Ryu, J.J. Park, J.-I. Baek, C.K. Ryu, J.C. Kim, Korean J. Chem. Eng. 28 (2011) 480–486.
- [27] L. Stevens, K. Williams, W.Y. Han, T. Drage, C. Snape, J. Wood, J. Wang, Chem. Eng. J. 215–216 (2013) 699–708.
- [28] N. Álvarez-Gutiérrez, M.V. Gil, F. Rubiera, C. Pevida, Chem. Eng. J. 307 (2017) 249–257.
- [29] S. Lagergren, Handlingar 24 (1898) 1-39.
- [30] E.C.N. Lopes, F.S.C. dos Anjos, E.F.S. Vieira, A.R. Cestari, J. Colloid Interf. Sci. 263 (2003) 542–547.
- [31] C. Zhao, X. Chen, C. Zhao, Ind. Eng. Chem. Res. 51 (2012) 14361–14366.
- [32] P.K. Gbor, C.Q. Jia, Chem. Eng. Sci. 59 (2004) 1979–1987.
- [33] N. Querejeta, M.V. Gil, C. Pevida, T.A. Centeno, J. CO<sub>2</sub> Util. 26 (2018) 1–7.
- [34] H. Wei, S. Deng, B. Hu, Z. Chen, B. Wang, J. Huang, G. Yu, ChemSusChem 5 (2012) 2354–2360.
- [35] Z. Zhang, J. Zhou, W. Xing, Q. Xue, Z. Yan, S. Zhuo, S.Z. Qiao, Phys. Chem. Chem. Phys. 15 (2013) 2523.
- [36] J. Šerafin, U. Narkiewicz, A.W. Morawski, R.J. Wróbel, B. Michalkiewicz, J. CO<sub>2</sub> Util. 18 (2017) 73–79.
- [37] J.P. Marco-Lozar, M. Kunowsky, F. Suárez-García, A. Linares-Solano, Carbon 72 (2014) 125–134.
- [38] B. Adeniran, E. Masika, R. Mokaya, J. Mater. Chem. A 2 (2014) 14696
- [39] H. Luo, H. Chioyama, S. Thürmer, T. Ohba, H. Kanoh, Energy Fuels 29 (2015) 4472–4478.
- [40] C. Zhao, X. Chen, C. Zhao, Energy Fuels 26 (2012) 1401–1405.
- [41] C. Zhao, X. Chen, C. Zhao, Ind. Eng. Chem. Res. 49 (2010) 12212–12216.
- [42] S. Freguia, G.T. Rochelle, AIChE J. 49 (2003) 1676–1686.
- [43] T. Neveux, Y. Le Moullec, J.P. Corriou, E. Favre, Chem. Eng. Trans. 35 (2013) 337–342.
- [44] G. Puxty, R. Rowland, A. Allport, Q. Yang, M. Bown, R. Burns, M. Maeder, M. Attalla, Environ. Sci. Technol. 43 (2009) 6427–6433.
- [45] L. Dubois, D. Thomas, Chem. Eng. Technol. 35 (2012) 513-524.
- [46] S.C. Lee, J.C. Kim, Catal. Surv. Asia 11 (2007) 171-185.
- [47] S.C. Lee, B.Y. Choi, T.J. Lee, C.K. Ryu, Y.S. Ahn, J.C. Kim, Catal. Today 111 (2006) 385–390.
- [48] Y. Guo, C. Li, S. Lu, C. Zhao, Chem. Eng. J. 301 (2016) 325–333.
- [49] Y. Guo, C. Li, S. Lu, C. Zhao, Chem. Eng. J. 308 (2017) 516-526.

- [50] I. Durán, F. Rubiera, C. Pevida, J. CO<sub>2</sub> Util. 26 (2018) 454–464.
  [51] M.G. Plaza, A.S. González, C. Pevida, F. Rubiera, Fuel 140 (2015) 633–648.
  [52] D.D. Do, H.D. Do, Sep. Purif. Technol. 20 (2000) 49–65.
- [53] G. Song, X. Zhu, R. Chen, Q. Liao, Y.-D. Ding, L. Chen, Chem. Eng. J. 283 (2016) 175–183.

- 175-183.
  [54] B.H. Hameed, I.A.W. Tan, A.L. Ahmad, Chem. Eng. J. 144 (2008) 235-244.
  [55] L. Ai, M. Li, L. Li, J. Chem. Eng. Data 56 (2011) 3475-3483.
  [56] M.H. Kalavathy, T. Karthikeyan, S. Rajgopal, L.R. Miranda, J. Colloid Interface Sci. 292 (2005) 354-362.
  [57] R. Serna-Guerrero, A. Sayari, Chem. Eng. J. 161 (2010) 182-190.
  [58] B. Royer, N.F. Cardoso, E.C. Lima, J.C.P. Vaghetti, N.M. Simon, T. Calvete, R.C. Veses, J. Hazard. Mater. 164 (2009) 1213-1222.

- [59] A.R. Cestari, E.F.S.S. Vieira, G.S. Vieira, L.E. Almeida, J. Hazard. Mater. 138 (2006) 133-141.
- [60] A.R. Cestari, E.F.S. Vieira, J.D.S. Matos, D.S.C. Dos Anjos, J. Colloid. Interface Sci. 285 (2005) 288–295.
  [61] E.W. de Menezes, E.C. Lima, B. Royer, F.E. de Souza, B.D. dos Santos, J.R. Gregório, T.M.H. Costa, Y. Gushikem, E.V. Benvenutti, J. Colloid. Interface Sci. 378 (2012) 10–20.